

Early development and tuning of a global coupled cloud resolving model, and its fast response to increasing CO₂

Thorsten Mauritsen^{1*}, Rene Redler², Monika Esch², Bjorn Stevens², Cathy Hohenegger², Daniel Klocke², Renate Brokopf², Helmuth Haak², Leonidas Linardakis², Niklas Röber³,
Reiner Schnur²

May 10, 2022

This is a non-peer reviewed manuscript

¹ Meteorologiska Institutionen vid Stockholms Universitet (MISU), Stockholm, Sweden

² Max Planck Institut für Meteorologie (MPI-M), Hamburg, Germany

³ Deutsches Klimarechenzentrum GmbH (DKRZ), Hamburg, Germany

* Corresponding author: Thorsten Mauritsen, e-mail: thorsten.mauritsen@misu.su.se

Since the dawn of functioning numerical dynamical atmosphere- and ocean models, their resolution has steadily increased, fed by an exponential growth in computational capabilities. The computationally limited resolution of models means that a number of mostly small-scale or micro-scale processes have to be parameterised – in particular those of atmospheric moist convection and ocean eddies are problematic when scientists seek to interpret output from model experiments. Here we present the first coupled ocean-atmosphere model experiments with sufficient resolution to dispose of moist convection and ocean eddy parameterisations. We describe the early development and discuss the challenges associated with conducting the simulations with a focus on tuning the global mean radiation balance in order to limit drifts. A four-month experiment with quadrupled CO₂ is then compared with a ten-member ensemble of low-resolution simulations using MPI-ESM1.2-LR. We find broad similarities of the response, albeit with a more diversified spatial response with both stronger and weaker regional warming, as well as a sharpening of precipitation in the inter tropical convergence zone. These early results demonstrate that it is already now possible to learn from such coupled model experiments, even if short by nature.

1 Introduction

Modern coupled ocean-atmosphere climate modeling has its roots in the idea that one can simulate the motion of the atmosphere and oceans using the laws of physics. This idea in turn dates back more than a century when Bjerknes (1904) first proposed weather forecasting as an initial value problem. His idea was quickly followed up by Richardson (1922) in his seminal attempt to calculate a short weather forecast by hand. With the advent of computers such simulation became applicable to both weather forecasting as well as climate modeling in the 1950's and 1960's (Charney et al., 1950; Bolin, 1955; Phillips, 1956; Manabe et al., 1965; Manabe and Bryan, 1969). A limitation of

Clouds and sea surface temperature

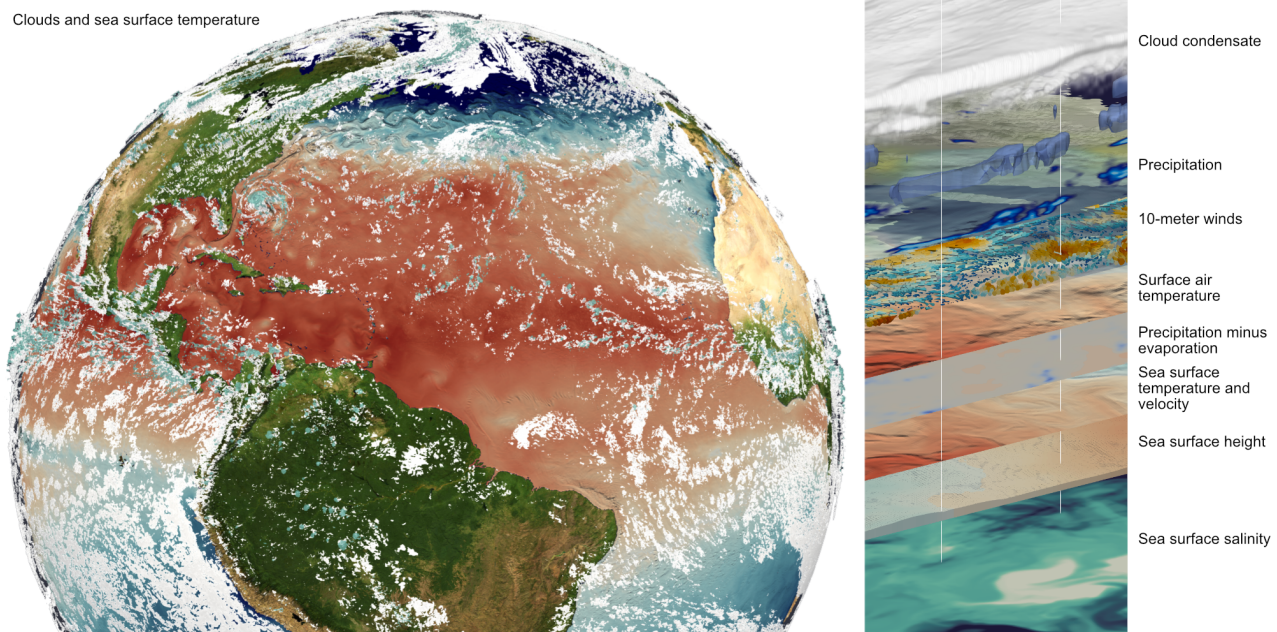


Figure 1: Snap shot of sea surface temperature and clouds in the coupled ICON-Sapphire experiments. Left is the North Atlantic region with sea surface temperatures displayed in colors from warm (red) to cold (blue) and a three-dimensional volume rendering of clouds. To the right is a layered display of various variables in the model. Note that several of these are defined at the surface.

climate modeling is that important small scale motion, not resolved by the computational grid, must be parameterised which is a leading source of uncertainty and a limitation to our ability to understand the results. In this paper we describe the development of a coupled climate model with sufficient resolution to represent atmospheric moist convection, gravity wave drag and ocean eddies and so can dispose of their parameterisations (Fig. 1).

Climate modeling as an activity on its own has not come far over the past five decades in answering basic questions such as how much warmer the planet might be on average at the end of this century (Zelinka et al., 2020; Flynn and Mauritsen, 2020), and likewise progress on representing regional information on societally important quantities such as precipitation change has been close to non-existent (Shepherd, 2014; Fiedler et al., 2020). A common approach in the community is to further increase the complexity of models and to elaborate their parameterisations (Washington et al., 2008). Although such continual refinement may help to better fit aspects of the observed climate, and these types of models will undoubtedly remain useful tools for decades to come (Balaji et al., 2022), the idea that major breakthroughs are to be expected has been challenged (Palmer and Stevens, 2019). Another recent idea is to replace the model parameterisations with machine learning algorithms (Schneider et al., 2017), though this has still to be demonstrated in actual experiments. Furthermore, testing and interpreting results from such models on the climate change problem may prove challenging.

A more transparent approach, the one which we favor here, is to dramatically increase the model grid resolution to the point where parameterisations can be reduced in number, and for those that inevitably remain more accurate versions can be chosen. There is vast experience that this physics-

46 based approach can be fruitful from studies of limited area simulations, or stand alone atmosphere
or ocean models (e.g. Deardorff, 1970; Klemp and Wilhelmson, 1978; Smith et al., 2000; Tomita et al.,
48 2005; Heinze et al., 2017; Stevens et al., 2019). In particular horizontal ocean eddies, moist convection
and various forms of gravity wave drag are for the most part parameterised in contemporary climate
50 models, but at kilometer scale resolutions the effect of these processes can largely be represented
by resolved motion. That is not to say that these processes are by any means fully resolved when
52 using such a grid, rather our claim is that a distorted representation of a physical process, one based
on the solution of the basic equations that govern it, is often a better solution.

54 We will argue that the time to develop global cloud resolving climate models is now. Experimentation
with such models is by and large limited by the number of years that can be simulated on
56 computers available to scientists in a given amount of real time, also referred to as throughput, or
temporal compression, typically measured in days per day or years per day. Today, practical imple-
58 mentations divide the problem into smaller pieces that are then calculated in parallel on individual
compute cores that then exchange data to solve the global problem. The maximum throughput
60 that can be attained at a given resolution if the number of cores is infinite is limited foremost by
time-step length, the speed of individual cores, and communication (Amdahl, 1967). For the ICON
62 model and a recently retired computer architecture we estimate the theoretical maximum through-
put and also display a series of real world examples (Fig. 2). The maximum throughput limit can
64 be increased, although not dramatically. The experiments with ICON discussed in this paper were
done at a throughput of about 17-30 days per day depending on configuration, although in practice
66 only a fraction of this because the simulations had to queue on the computer, and as such these
experiments were at the limit of what was feasible for us to do up to now. Nevertheless, with the
68 rapidly decreasing cost of compute resources (Moore, 1965), such simulations are going to become
more common in the coming years.

70 Also, technical innovation, such as the use of graphics processing units (GPU) can accelerate this
progress (Yashiro et al., 2016; Fuhrer et al., 2018); a current example from ICON is given in Figure
72 2. These GPU-based simulations will have a lower maximum throughput due to their inherent
parallelism and low per-core performance. The example given is close to the maximum throughput
74 at 2.5 km resolution, about a factor 4-5 below the theoretical maximum throughput with CPUs. To
achieve the corresponding throughput to these 2048 GPUs, however, we estimate we would need
76 about 1 million CPU cores, an amount which is currently only available on a few machines world
wide. As such GPUs present an advantage over CPUs on these large problems that are limited by
78 the available memory and computing power.

Although experimentation with globally coupled cloud-resolving models in the 2020s will for
80 the most part be limited to decades, and one must dismiss the idea of eliminating long term cli-
mate drifts through millennia long spin-ups such as is commonly applied to current climate models
82 (Mauritsen et al., 2012; Hourdin et al., 2017), there is still a wealth of interesting experiments that
can be conducted and phenomena that can be studied which were not feasible before. What is
84 more, due to the maximum throughput limitation, these simulations will probably not be able to
run at more than a few years per day within the foreseeable future, such that their scope to study
86 timescales longer than a few hundred years is inherently limited, i.e. that which can be computed

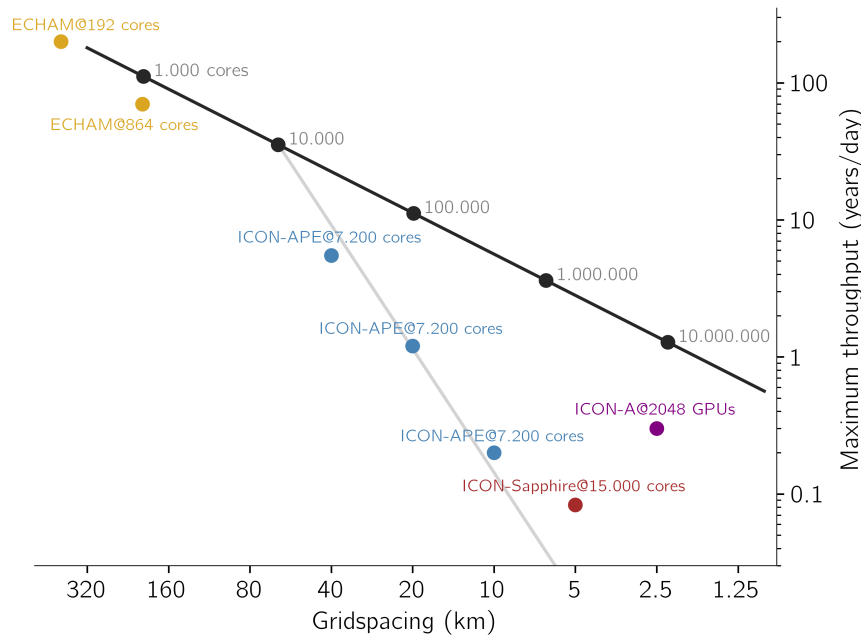


Figure 2: The maximum throughput in years per day as a function of horizontal grid spacing. Thick black line is the estimated maximum with recent technology, here the Intel Xeon E5-2695V4 Broadwell processor based Mistral supercomputer built 2015 at the Deutsches Klimarechenzentrum (DKRZ). Dots and numbers along that line indicates the approximate number of compute cores needed to reach that level of performance as extrapolated from the low-resolution experiments. Grey line shows the approximate performance for a given number of cores at increasing resolutions, as can be compared with the blue symbols: Yellow and blue symbols are for ECHAM6.3 and ICON atmosphere-only experiments carried out in 2017 without output, whereby ICON-A and ECHAM6.3 experiments were with continents and ICON-APE is idealised aquaplanet experiments. The brown symbol is for the coupled ocean-atmosphere ICON-Sapphire configuration as used in this study with twice as many levels as the aquaplanet experiments and asynchronous output. This coupled model run contains many optimisations over the earlier ICON-APE experiments, but also dedicate compute cores to an ocean and is hampered by some load unbalancing. Purple symbol is an atmosphere only experiment that has been ported to using Nvidia A100 Graphics Processing Units (GPUs) on the Jülich JUWELS Booster supercomputer.

in a year. Hence, we argue, the time to develop, apply and exploit these new tools is now.

88 In the following we will share our experience with developing ICON into a cloud- and ocean eddy
resolving model that resulted in multiple year-long simulation, and thereafter we shall investigate
90 the models surface temperature and precipitation response in the first four months following a
quadrupled atmospheric CO₂ concentration, providing an example of how such models can already
92 now be used to gain understanding.

2 Model developments

94 The purpose of the here described project, launched in the winter 2017/18, was to demonstrate that
coupled simulations with sufficient resolution to explicitly represent moist deep convection and
96 ocean eddies are now both feasible and useful. As such the purpose was not in the first place to
achieve fidelity with observations in all respects, but first and foremost to show that already now
98 it is possible to experiment with a coupled ocean-atmosphere model at this level of resolution. To
this end, we decided to aim for running an annual cycle simulation during the project, and in ad-
100 dition it was decided to explore the model response to increasing CO₂. ICON is developed in a few
different configurations, for instance to support numerical weather prediction (ICON-NWP), or as
102 a traditional CMIP class model (ICON-ESM). The model version to be developed here was named
ICON-Sapphire, with reference to the gems blue colour, signifying the focus on fine-scale resolu-
104 tion. In this publication we focus on describing the process of the early developments, whereas a
complete description of the ICON-Sapphire modeling system and its many other capabilities, as
106 they developed out of this and other projects, is given in a companion paper (Hohenegger et al.,
2022).

2.1 Strategy

To achieve this goal a pragmatic approach was taken – something we came to refer to as ”the work-
110 bench” – whereby existing model components were first brought together to a setup that could
actually run, even if only for a few time steps before the computation would fail. Thereafter, prob-
112 lems could be identified and amended as they would become apparent. New developments could
then be tested in an already working coupled setup. But overall progress of the project did not hinge
114 on a single development. Insofar that it was possible, the latest setup of the model was kept run-
ning on the computer at all times to gather information about both technical issues, computational
116 performance and physical biases.

The chosen development strategy was computationally expensive. The coupled simulation re-
118 quired a minimum of 15.000 computational cores of the total 100.000 cores available on the DKRZ
Mistral supercomputer in order to fit in the systems memory. This represented a tremendous insti-
120 tutional investment as the Max Planck Institute has access to about half the computer, and so the
development had to be weighed against displaced ongoing research also taking place on the same
122 allocation. To hedge against the high development cost, both uncoupled atmosphere-only (5 km)
and lower resolution coupled (160 km) setups were used extensively for testing. Although these

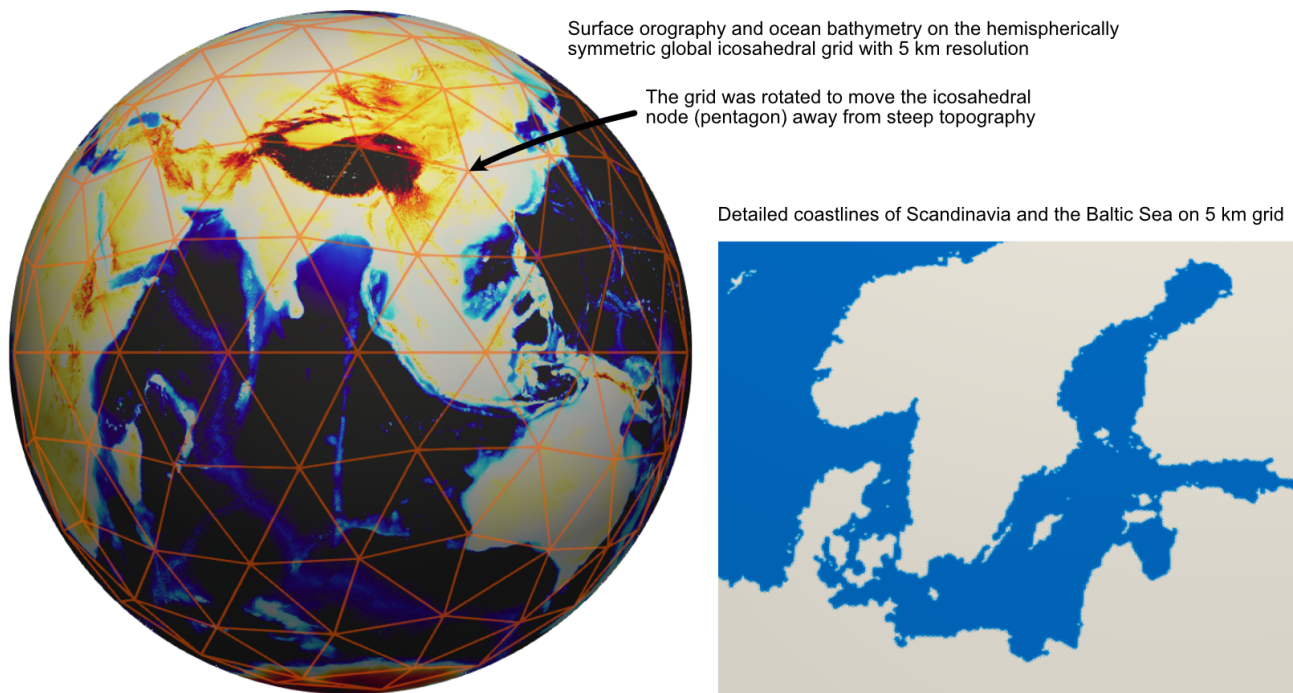


Figure 3: Illustrations of the global hemispherically symmetric 5 km resolution grid used here. Left is a global view of the ocean bathymetry and land orography. Also shown as red lines is the first refinement of the basic icosahedral grid. Note how this version of the grid is stretched to be symmetric about the equator in order to minimise imprints on tropical ocean dynamics, and also how the nodes of the original icosahedron that are surrounded by a pentagon are shifted away from the steep orography of the Himalayas. On the right is shown a zoom of the details of coastlines around the Baltic Sea.

124 setups could be used for a number of purposes, some of the problems we faced would only show up
 125 in the high resolution coupled setup, and so also gaining experience running this more expensive
 126 setup was indispensable to the development.

2.2 Matching ocean and atmosphere grids and their coupling

128 In the spirit of keeping things simple, it was decided to use matching grids in the atmosphere
 129 and ocean. This approach eliminates the need to interpolate during coupling and simplifies the
 130 handling of coastlines. The grid of ICON is based on the icosahedron (Sato, 2014), which consists
 131 of 20 triangles projected onto the sphere (Figure 3). The sides of the triangles are bisected to form
 132 smaller triangles to achieve the desired resolution. To save system memory the land grid points in
 the ocean model were excluded.

134 Several measures were taken to make the grid more uniform and improve the dynamics of the
 135 model. The triangles near the corners of the original icosahedron form a pentagon, rather than a
 136 hexagon (Figure 3), and their edges are the shortest by default. To reduce this grid distortion of
 the grid a spring dynamics optimisation is applied (Tomita et al., 2001, 2002), leading to reduced
 138 numerical errors (Weller et al., 2009; Korn and Linardakis, 2018). Furthermore, out of experience
 it can cause numerical instabilities, resulting in model crashes, if these points are placed on steep
 140 orography. Therefore it was decided to rotate the grid by 37 degrees to move such a point out of

the Himalayas (Figure 3). Finally, the grids were symmetrised with respect to the equator (Heikes
142 and Randall, 1995a,b), which has been found to improve the modelled ocean dynamics (Korn and
Linardakis, 2018) and in preliminary tests with an aquaplanet setup to reduce the frequency of high
144 horizontal Courant-Friedrich-Lewy (CFL) number events in the atmosphere, thereby permitting a
slight increase in the time step length.

146 The ocean and atmosphere model components run concurrently and perform a parallel data
exchange. The number of compute processes for the atmosphere and ocean are determined in-
148 dependently, and as a consequence we do not have a one-to-one relation between the ocean and
atmosphere processes. To handle the exchange at the ocean-atmosphere interface we use the YAC
150 coupling library (Hanke et al., 2016; Hanke and Redler, 2019). The interpolation capabilities of YAC
are not used here, as due to the matching grids a simple nearest-neighbor search to handle the
152 repartitioning is performed during the initialisation. This search takes roughly 5 seconds. During
the run, the coupling routines are called at every model time step, whereby surface exchange data
154 are collected. At user-defined coupling events - here every 900 seconds - the data is averaged and
sent to the respective receiving processes in the atmosphere and ocean. The resulting coupling
156 performance is satisfactory and scales well.

In practice, the setup led to a substantial load imbalance. This happened because at a given
158 resolution the ocean can take longer time steps (120s) than the atmosphere (30-45s), but the mem-
ory usage is similar: The ocean would fit in memory with 120 compute nodes, each containing
160 36 compute cores and 64 GB memory; for the atmosphere this memory limitation was 150 nodes.
The memory bottleneck of the ocean was related to the output mechanism used by the ocean, and
162 this issue has later been addressed. In practice the size and total load on the machine meant we
would not request more than 300 nodes for the atmosphere. Consequently, the ocean was waiting
164 for the atmosphere at each coupling event. With a larger machine the load imbalance could be
easily eliminated since the ICON atmosphere is far from scaled out at 5 km resolution (Figure 2,
166 ICON-Sapphire is well below the black line).

2.3 Experiment overview

168 The development of the physical model improvements could in retrospect be described as having
happened along major development steps, which were characterised by being run longer, comple-
170 mented by shorter intermediate tests. As described above the strategy was to start with something
that works, here the recently developed ICON-ESM (Giorgetta et al., 2018), and then incremen-
172 tally move towards the goal of a coupled model with parameterisations that are suitable for cloud
resolving simulations at kilometre or finer scales.

174 In defining our goal, we took inspiration from both large-eddy simulations (LES) and cloud re-
solving models (CRMs), which are both widely used on limited area domains, and we decided to
176 aim at having an advanced cloud micro physics parameterisation (Baldauf et al., 2011), combined
with a three-dimensional turbulence mixing scheme (Dipankar et al., 2015). The latter was not intro-
178 duced from the start since it was still in development, see below. Likewise, the partial cloud fraction
scheme Sundqvist et al. (1989) was replaced with a simple binary cloud fraction. The convection

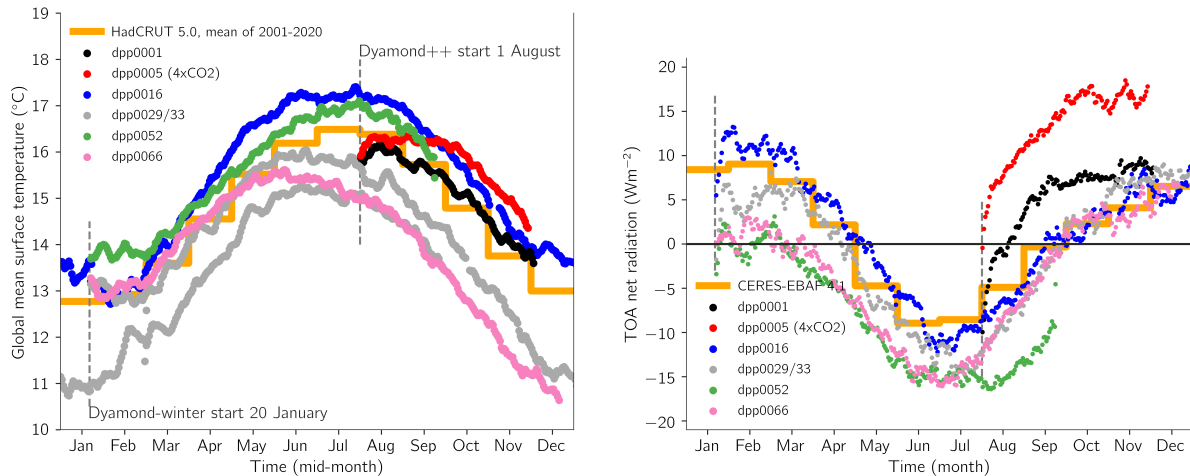


Figure 4: Evolution of temperature and radiation balance with time in the coupled simulations. Left panel shows daily global mean temperature in simulations compared with the average annual cycle from HadCRUT 5.0 reconstruction averaged over the 2001-2020 period. Starting dates of the experiments are marked with vertical dashed lines. The right panel shows the top of atmosphere radiation balance compared to monthly mean observed radiation balance from CERES-EBAF edition 4.1 averaged over the 2001-2020 period. Note that the right panel only shows the first year of dpp0029/33, and also that dpp0005 has quadrupled CO_2 and so is therefore not expected to match observations.

180 (Tiedtke, 1989) and gravity wave drag (Lott, 1999) parameterisations were turned off because these
 182 processes are assumed to be resolved by the equations of motion. In retrospect the development
 could be viewed as having had three phases:

1. Early experiments focused on technical coupling and computational performance
- 184 2. Replacement of cloud microphysics (dpp0001/5, dpp0016)
3. Replacement of turbulent mixing scheme (dpp0029/33, dpp0052, dpp0066)

186 Here the experiment names are "dpp" after DYAMOND++, in turn named after the DYNAMICS of
 the Atmospheric general circulation Modeled On Non-hydrostatic Domains (DYAMOND) project
 188 (Stevens et al., 2019), '++' referring to this being coupled to the oceans rather than using prescribed
 sea surface temperatures and sea ice distributions, followed by a number in the series of experi-
 190 ments. Each experiment is described in more detail in Table 1. An overview of the temperature
 and radiation imbalance evolution in the experiments is displayed in Figure 4, and maps of surface
 192 temperature biases in Figure 5.

2.4 Model initialisation

194 In the first experiments with the new model setup, we often experienced numerical instabilities
 in the early stages of the simulation caused by large gravity waves in the ocean. The ocean was
 196 initialised from a climatology which did not have a dynamically balanced surface circulation. There-
 fore we undertook a 10 year ocean-only simulation at 10 km resolution with initial conditions from

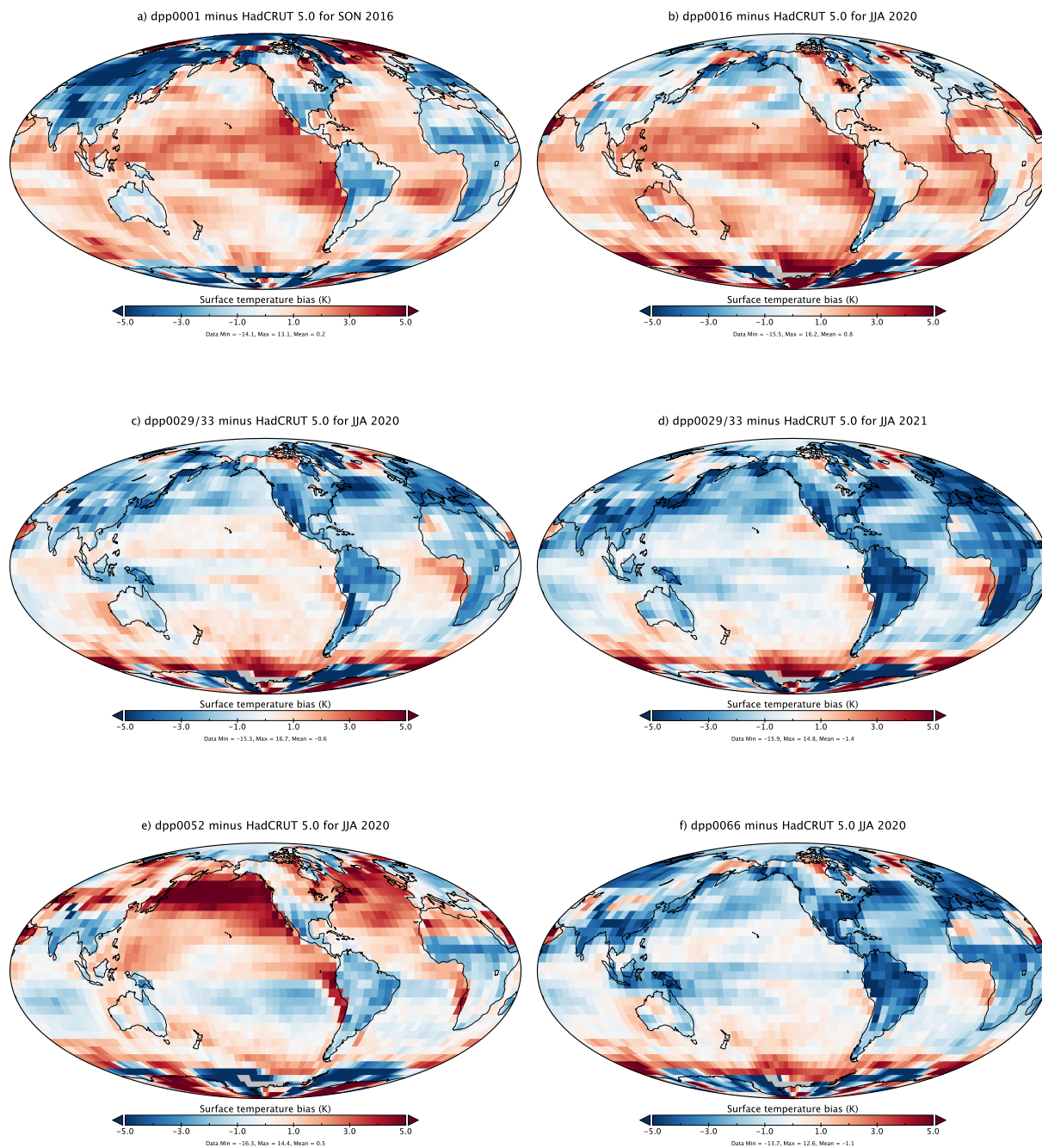


Figure 5: Surface temperature biases for June to August relative to HadCRUT 5.0 averaged over the years 2001-2020. Note that panel a) shows September to November (SON), whereas the other panels are June to August (JJA). Panels c) and d) shows the bias in the first and second year of the dpp0029/33 experiment.

Table 1: Overview of experiments conducted during the project.

Experiment ID	Description
dpp0001:	The first working model was based on existing components from ICON-ESM, but with advanced cloud micro physics, convection and gravity wave drag parameterisations turned off, and using a binary cloud fraction scheme. The model was still using the total turbulent energy mixing scheme (Pithan et al., 2015). The experiment was started 1 August 2016 and ran with multiple numerical crashes starting in November until 19 December.
dpp0005:	In the companion experiment to dpp0001 the atmospheric CO ₂ was quadrupled (see Section 3).
dpp0016:	To reduce the model warming drift the average ocean surface albedo was raised from 7 to 12 percent (Section 2.5). Also various technical improvements were made to reduce the numerical instabilities. This permitted us to raise the model top from 30 to 75 km. The experiment was started on 20 January 2020, and ran for one year.
dpp0029/33:	In the third step we replaced the total turbulent energy mixing scheme with the Smagorinsky three dimensional turbulence scheme. Furthermore we improved the coupling between winds and ocean currents. The run has substantially more clouds, so the ocean albedo was again reset to its default. In addition the cloud inhomogeneity factor was reduced from 1 to 0.66 to reduce solar reflection. The dpp0029 simulation was started on 20 January 2020 and after reaching one year it was extended as dpp0033 by another 9 months using more vertical resolution in the ocean.
dpp0052:	In this update a programming error in the surface sensible heat flux calculation was removed and a new ocean vertical coordinate introduced. The tuning parameters were kept the same as in dpp0029/33.
dpp0066:	In this update the new ocean vertical coordinate introduced in dpp0052 were removed again in order to separate its effect from other changes. The tuning parameters were again kept the same as in dpp0029/33.

198 the 30 km ORAS5 ocean reanalysis and surface boundary conditions from the ERA-5 atmosphere
reanalysis. The resulting state of the ocean was then interpolated to 5 km resolution, and the spin
200 up continued for another 10 years. Although costly, the method resulted in an initial state with
balanced ocean eddies, and furthermore we experienced fewer model crashes after the ocean was
202 coupled to atmosphere.

The atmosphere was initialised from an ECMWF operational analysis on the initial time and
204 day of the experiment. For dpp0001 this was 00 UTC on 1 August 2016 as in Stevens et al. (2019),
whereas in the other experiments a starting date of 20 January 2020 was chosen to match the
206 start date of the EUREC4A field campaign (Bony et al., 2017; Stevens et al., 2021). The initial data
for land soil moisture and temperature of the 5 soil layers as well as snow cover are the same as
208 used in the MPI-ESM1.2 model and were simply interpolated to the ICON grid. The procedure
was refined in simulations subsequent to dpp0029/33 to instead use soil moisture, soil temperature
210 and snow fields from the same ECMWF analysis with which the atmospheric state is initialised.
It is not obvious which approach is better, though, since in both cases these are modelled fields
212 from modeling systems likely to exhibit different snow and soil moisture climates to that of ICON-
Sapphire. Thus a drift in these fields during the first years of simulation is inevitable.

214 **2.5 Tuning experience, drifts and biases**

Drifts in the global mean temperature of coupled climate models is commonly controlled by tuning
216 the radiation balance followed by long spin-ups of typically several thousands of years (Hourdin
et al., 2017). If the radiation balance is not tuned the surface temperature will drift away from the
218 observed, thereby making it more challenging to exploit the model for scientific purposes. Tuning is
typically done by adjusting various model parameters, mostly pertaining to cloud processes which
220 tend to be effective in controlling the radiation balance. Furthermore, this tuning can also be used
to compensate energy leakages in climate models, which are often on the order of 5 Wm^{-2} , by
222 maintaining a correspondingly compensating top of atmosphere radiation imbalance (Mauritsen et
al., 2012). There are, however, particular issues to consider when minimising drift in a global cloud
224 resolving model. Here we provide our experience, in the hope that other groups pursuing global
coupled cloud resolving models may benefit.

226 **2.5.1 Tuning parameters**

The parameters used in climate model tuning are usually considered uncertain due to issues with
228 representing small scale cloud processes at grid spacing of the order of hundred kilometers, and
thereby justified as tunable parameters. At kilometer scale resolutions, however, these uncertain-
230 ties are substantially reduced such that one might question the justification. Furthermore, because
we turn off the convection scheme in order to instead explicitly resolve convection, a number of pa-
232 rameters that are typically used for tuning are consequently lacking. With fewer and less uncertain
parameters at disposal, we may have to resort to using parameters outside their respective ranges
234 of uncertainty, or parameters not usually used for tuning. As an example we used ocean surface
albedo to tune dpp0016 colder relative to the warm-biased dpp0001. Although such measures are

not justified by an imperfect knowledge of the ocean surface albedo, it may still be justified to do such tuning in order to limit model drift, here caused by a lack of low-level clouds.

Tuning parameters may not always work the way they used to do at lower resolutions. We encountered such an example during the pre-dpp0001 phase with the relative humidity based fractional cloud cover scheme. In this scheme a critical relative humidity profile, usually 70–90 percent, determines at which large-scale relative humidity clouds start to form; a lower value means more clouds and usually has a cooling effect. We initially set this to 100 percent in our experiments to yield an all-or-nothing scheme, but when we were faced with too few low level clouds in early versions (Phase 1, Section 2.3), we tried to lower the value. To our surprise this led instead to even fewer clouds. Since this route was anyway not aligned with our long term vision we did not investigate the cause further. We speculate, however, that lowering the threshold for cloud formation could cause resolved convection to trigger more easily, leading to a drying of the atmosphere.

2.5.2 Informative short runs

To gain experience with the tuning parameters we found it useful to analyse short initialised atmosphere only runs. Usually, when tuning the contemporary climate model MPI-ESM1.2 we run the model in atmosphere only configuration for years or decades to get a good estimate of the parameters effects while averaging over internal variability. An alternative is to use short initialised runs, wherein weather events are nearly the same (Wan et al., 2014). These runs need to be shorter than the weather prediction limit of about two weeks (Lorenz, 1969), so we decided to use 5-day simulations which ensures similar synoptic scale weather.

We primarily used such short runs to determine how strong the effect of a certain parameter change is on the global mean radiation balance. Since the parameters we used for tuning were either related to cloud processes, or the ocean surface albedo, which have either fast or instantaneous effects our experience was that we were able to obtain a reasonable estimate of their longer term effects based on 5-day simulations.

However, the short runs were also useful in a more qualitative sense. In Figure 6 we compare a satellite image of the longwave brightness temperature, estimated by combining multiple channels, with that which the satellite would have seen in two versions of the ICON model. First, we note a striking similarity: convective clouds are in roughly the right places. But both model versions exhibit smaller convective clouds with less of the thin anvil seen as a light gray veil over central Africa in the satellite image. This was more pronounced in the ICON version shown in panel b) which still used the diagnostic cloud micro physics. The comparison motivated the move to the prognostic scheme used in the numerical weather prediction version, ICON-NWP (panel c). We also noted the box-shaped anomaly near Morocco which was caused by an error in the surface boundary conditions.

2.5.3 Controlling drift

Contemporary climate models are typically spun up to reach a stationary state before experimentation starts, however, it is not practical to make such long spin up runs with coupled cloud resolving

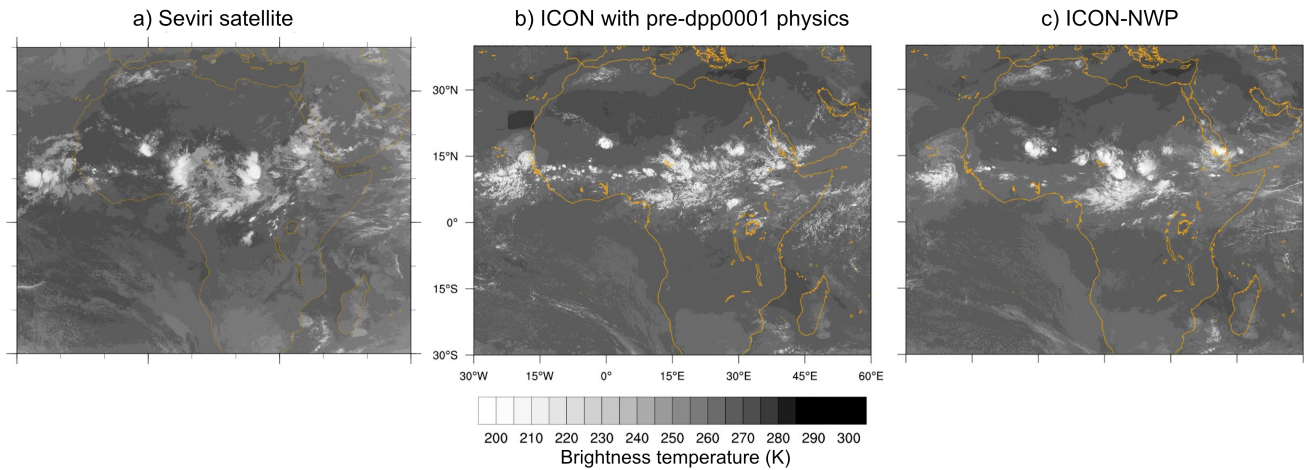


Figure 6: Comparison of infrared brightness temperature observed from the Seviri weather satellite (a), with 12-hour initialised runs from an early version of ICON-Sapphire with diagnostic cloud micro physics (b), and with the numerical weather prediction (NWP) physics package that includes prognostic cloud micro physics used by the German Weather Service (DWD) (c).

274 models. Even if eventually in a few decades, it will no longer be nearly as computationally expensive
 275 to run these models, they are still going to be inherently slow, and so it will take years of real time
 276 to perform a spin up anywhere nearly long enough to eliminate drifts. Consequently, in addition
 277 to limit drifts caused by a biased radiation balance, the development should aim at also reducing
 278 initial model drifts which is perhaps a more challenging task.

If we assume that the model conserves energy, then we can combine the modelled global mean
 280 temperature and radiation balance (Fig. 4) to estimate how it will drift. For instance, dpp0001 ab-
 281 sorbs more radiation than observed, and consequently it will warm up with time, whereas dpp0029/33
 282 cools due to negative radiation balances. The tuned radiation balance of dpp0016 meant that it did
 283 not drift much. An interesting counter example is dpp0052 which has a negatively biased radiation
 284 balance, yet is warmer than observed; a case we shall discuss further below.

Estimating at which global mean temperature a model will drift towards is difficult based on
 286 short experiments. Here focus is often on the evolution of daily or monthly means (e.g. Fig. 4),
 287 but biases and drifts in these may result also from an erroneous representation of the annual cycle.
 288 From the longer dpp0029/33 experiment we can investigate this in more detail by plotting monthly
 289 mean radiation balance against surface temperature (Fig. 7). First we notice the observed evolution
 290 is shaped as an eight, presumable as surface temperature lags behind the radiation balance due to
 291 the heat capacity. The dpp0029/33 run, however, starts at lower radiation balance and hence drifts
 292 to colder temperatures, exhibiting a less obvious eight-shaped loop. Comparing the same months
 293 between the first and second year we see that the model drifts on a negative slope, consistent with
 294 an overall negative feedback (Mauritsen et al., 2012) which will eventually bring the model into bal-
 295 ance at a lower temperature. Based on these slopes we estimate the model will reach such balance
 296 for present day boundary conditions approximately 1.5 degrees below observed temperatures.

[The below needs revising, Rene Redler]

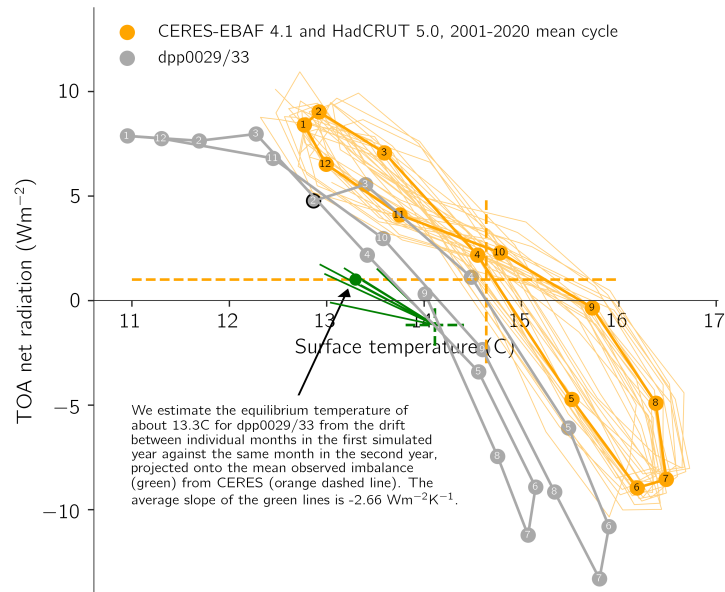


Figure 7: Evolution of temperature versus radiation balance in the two longest coupled simulations. Shown is the monthly mean temperature versus radiation balance for the two longer simulations and observations. Shown as thin orange lines are the 20 individual cycles of observations. Dashed orange lines are means of the observations, and as described within the figure we estimate the equilibrium temperature of dpp0029/33 from the drift between the two simulated years.

298 We encountered an interesting example wherein the radiation imbalance did not cause an im-
 300 mediate temperature drift in the experiment dpp0052 (Fig. 4); although the radiation balance is well
 302 below that observed by $5\text{-}10\text{ Wm}^{-2}$, the global mean surface temperature is about $0.5\text{-}1\text{ K}$ above
 304 the observed throughout the simulation. We were able to isolate this behavior to an issue with the
 306 updated vertical coordinate system in the ocean, by reverting only this change in dpp0066 (Table 1).
 Apparently, the fine vertical resolution permitted strong stratification in the uppermost meters of
 the ocean to develop in summer, which lead to suppressed turbulent mixing and therefore further
 stratification. The result is very large positive surface temperature biases in the summer hemisphere
 (Fig. 10e), explaining the unexpected evolution of the global mean temperature. Eventually, though,
 the oceans would have to cool in response to the negative radiation balance.

308 All in all, there are many new challenges associated with tuning the radiation balance and global
 mean temperature in global coupled cloud resolving models. But they are not insurmountable. Key
 310 to this will be to both build up an understanding of the role of the tunable parameters – here we
 have yet to familiarise ourselves with the new turbulence and cloud micro physics schemes – but
 312 also to eliminate structural problems such as energy conservation and other issues such as that
 encountered here with the ocean vertical mixing. Drifts can, however, not be eliminated entirely
 314 and users should be aware of this and take it into account in their analyses. Nevertheless, as the
 spin ups are short due to computational limitations, so are also the experiments that can be done
 316 with the model. Therefore the drifts that can be tolerated are much larger than with contemporary
 climate models.

318 2.5.4 Strikingly familiar sea surface temperature biases

Whereas the above has focused mostly on global mean temperature, we would like to also point
320 attention to the distribution of surface temperature biases (Fig. 10). First, one can distinguish
phase 2 runs with prognostic cloud micro physics which were dominated by warm biased tropical
322 sea surface temperatures (panels a and b), from phase 3 runs with the Smagorinsky turbulence
mixing scheme which instead are dominated by cold biased lands (panels c-f). Here dpp0052 (panel
324 e) sticks out due to the changed ocean vertical coordinate as discussed in the previous section.

Nevertheless, there are also interesting commonalities among the simulations: the warm bias in
326 the tropical eastern boundary up-welling stratocumulus dominated regions, the warm bias in the
Southern Ocean and the cold bias in the North Atlantic south of Greenland. All three regions are
328 also commonly biased in contemporary climate models. The warm bias in the stratocumulus regions
off the coasts of California, Peru, Namibia and Australia are thought to be a complex problem
330 combining too few clouds with erroneous coastal winds and ocean currents, some of which might
be helped by higher resolutions (Zuidema et al., 2016), though apparently they persist at 5 km grid
332 spacing. Presumably the coastal jets and ocean currents are well-resolved suggesting that instead
the poor representation of stratocumulus clouds which involve finer scales of motion is the main
334 source of error. The Southern Ocean warm bias is mostly due to issues with clouds (Hyder et
al., 2018). The Southern Ocean warm bias is not evident in dpp0001, but since it is analysed in
336 September to November, which is austral spring, it may be tied to sea ice melt in a way that the
other runs are not. The North Atlantic cold bias is commonly found in coupled climate models and
338 thought to be related to poorly represented ocean currents (Wang et al., 2014). It is intriguing that
these three long standing climate model biases remain at high resolutions, at least in the case of
340 ICON-Sapphire, suggesting that either even higher resolutions are necessary or that the remaining
physics parameterisations are the culprit.

342 3 Response to increasing CO₂

It is of particular interest to see if the response to increased atmospheric carbon dioxide (CO₂) of the
344 less parameterised ICON-Sapphire model compared to contemporary climate models. Although the
available run is insufficient to use the long-term response to probe the model's climate sensitivity,
346 it is possible to look at the fast response to CO₂. The fast precipitation response is a major part of the
long term response (Bony et al., 2013), and hence it is interesting whether the modeling approach
348 taken here leads to a different response. Furthermore, sea surface temperature patterns arising from
ocean heat uptake are thought to play an important role in setting the transient warming rate (Win-
350 ton et al., 2010; Held et al., 2010; Armour et al., 2013). Studies have suggested that contemporary
coupled climate models underestimate the strength of these patterns, and hence their dampening
352 effect, in particular by warming too fast in the East Pacific (Zhou et al., 2016). If this bias is related
to an inability of contemporary climate models to resolve ocean up-welling in the East Pacific, then
354 the response in the ICON-Sapphire runs should exhibit less warming in the region.

To investigate these ideas a four month simulation with ICON-Sapphire with quadrupled CO₂

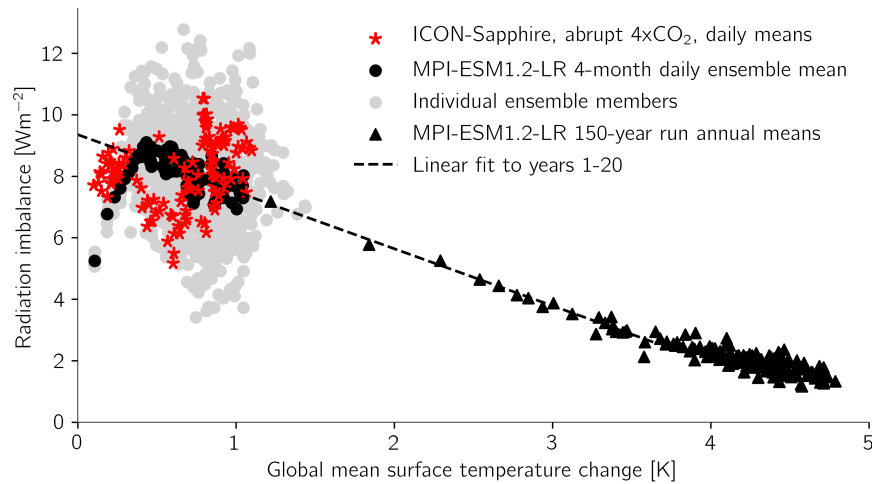


Figure 8: Top of atmosphere radiation balance versus global surface temperature in response to an abrupt quadrupling of atmospheric CO_2 . Shown as circles are daily means from 4-month simulations starting 1 August in a single realisation with ICON-Sapphire and ten realisations with MPI-ESM1.2-LR, as well as the ensemble mean of the latter. Triangles shows yearly means from a 150-year run. The dashed line is a linear fit to the latter run years 1-20.

356 starting on 1 August (dpp0005) is compared to an ensemble of simulations conducted with MPI-
 ESM1.2-LR (Mauritsen et al., 2019). This ensemble consists of 10 runs with quadrupled CO_2 also
 358 started on 1 August with initial conditions sampled from different years of a pre-industrial control
 simulation to sample internal variability. The response is then calculated as the difference relative to
 360 the control simulation over the corresponding period and/or region. As a result internal variability
 in both the quadrupled CO_2 experiment and the control impacts the result, compared to common
 362 practice where a long control simulation is averaged to eliminate internal variability. In our case,
 though, this effect is the same in both the ICON-Sapphire and the MPI-ESM1.2-LR experiments.

364 Scattering global means of surface temperature against top-of-atmosphere radiation balance is
 a common way to estimate forcing and feedback in climate models (Gregory et al., 2004). In the
 366 four months simulated here, both ICON-Sapphire and MPI-ESM1.2-LR warm by about 1 K and
 they exhibit similar radiation balances (Figure 8), as most of the daily means of ICON-Sapphire
 368 are within the ten member ensemble. The ensemble mean exhibits a short adjustment with rising
 radiation imbalance for a couple of weeks, as primarily the stratosphere cools, followed by a slow
 370 decline with further warming in line with the expected feedback as estimate by a linear fit to the
 first 20 years of a longer simulation. Thus, the high resolution ICON-Sapphire simulation global
 372 mean fast response is indistinguishable from that of the contemporary MPI-ESM1.2-LR climate
 model, and potentially the decadal feedback could be studied with just a few years of simulation
 374 in the near future.

Inspecting next the zonal mean surface temperature and precipitation response reveals a tem-
 376 perature response that is surprisingly similar between the two models (Figure 9). The ICON-
 Sapphire model is within the ensemble at most latitudes, albeit towards the least warming end
 378 in the sub-tropics south of the ITCZ (which is north of the Equator) and in the northern hemi-

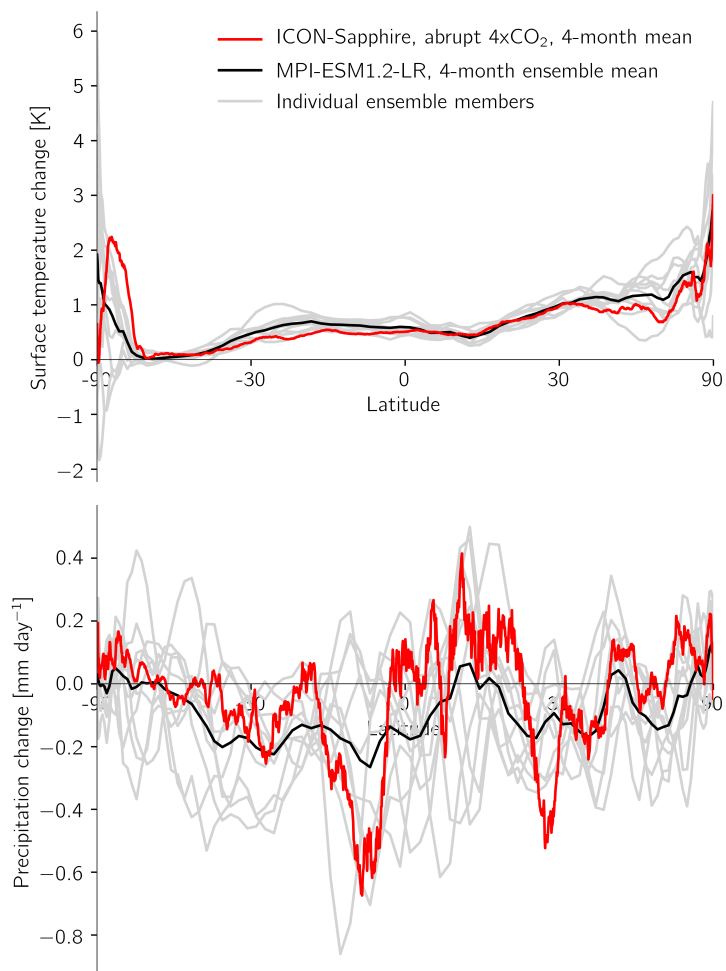


Figure 9: Zonal mean temperature and precipitation change in the first four months following a quadrupling of atmospheric CO₂.

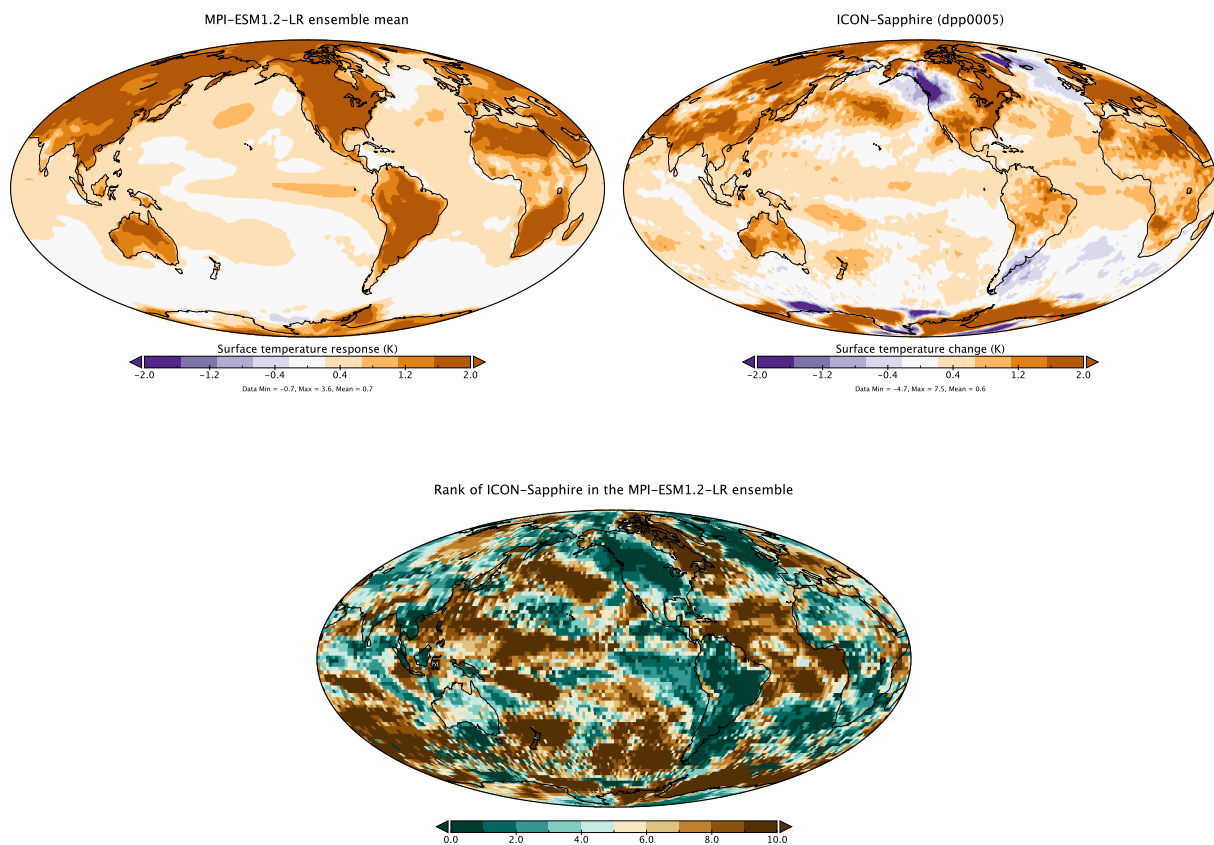


Figure 10: Mean temperature response during first four months following a quadrupling of atmospheric CO_2 . The upper left panel shows the 10-member ensemble mean from the MPI-ESM1.2-LR model and the right panel is from the ICON-Sapphire model, interpolated to the same T63 grid. The lower panel shows the rank of ICON-Sapphire in the MPI-ESM1.2-LR ensemble, whereby zero means it is the coldest and 10 means it is the warmest.

sphere mid-latitudes, and it warms the more than any ensemble member over part of the Antarctic.
 380 Zonal mean precipitation is more variable among the ten MPI-ESM1.2-LR ensemble members, and
 also here ICON-Sapphire lies mostly within the spread. Nevertheless, there is a systematic pattern
 382 with stronger increase of precipitation in the ITCZ region and strong decreases in the sub-tropics
 in the ICON-Sapphire simulation suggestive of a narrowing of the tropical rain band, even if the
 384 model is not an obvious outlier.

Returning to the surface temperature change, also the spatial structure of warming is similar
 386 between the MPI-ESM1.2-LR ensemble mean and the ICON-Sapphire response to quadrupled CO_2
 (Figure 10). There are regions where the response is different, for example cooling in the North
 388 Atlantic, in terms of the east-west gradient of warming in the tropical Pacific or generally less
 warming on land, however, it is to be expected that a single realisation contains more noise than
 390 an ensemble mean due to internal variability. To investigate this we calculate in each gridpoint
 the rank of ICON-Sapphire within the MPI-ESM1.2-LR ensemble: if ICON-Sapphire is coldest it is
 392 assigned rank 0, if it is the warmest rank 10. This confirms the impression from before, but also the

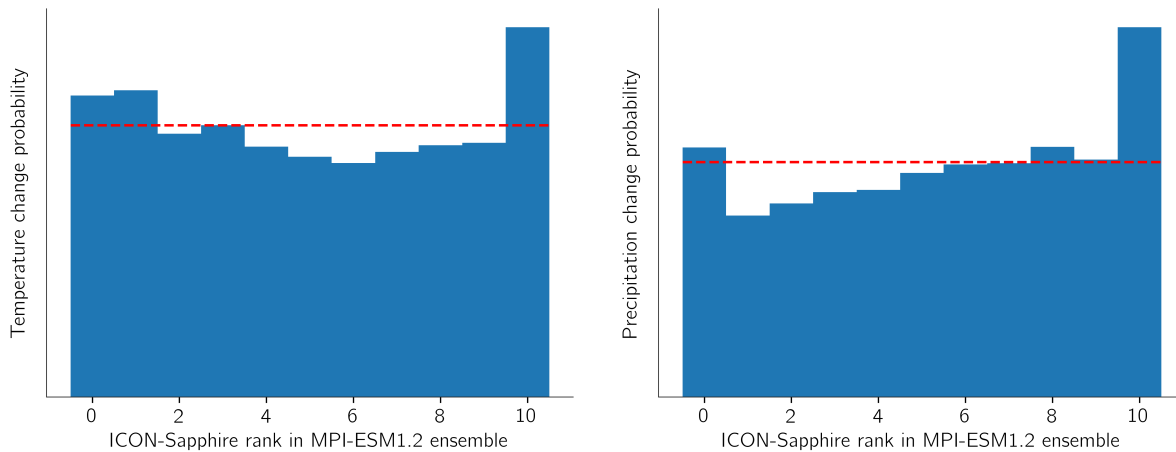


Figure 11: Rank histogram of temperature (left) and precipitation change (right) in ICON-Sapphire relative to the MPI-ESM1.2-LR ensemble in the first four months following a quadrupling of atmospheric CO₂, whereby zero means it is the coldest or driest and 10 means it is the warmest or wettest.

tropical Atlantic stands out with ICON-Sapphire ranking generally the highest. The corresponding rank histogram further shows that the surface temperature pattern of ICON-Sapphire is stronger than that of MPI-ESM1.2-LR with an over representation of ranks 0,1 and 10 (Figure 11). The map of precipitation rank is too noisy to be displayable, nevertheless the rank histogram of precipitation shows an over representation foremost of rank 10, which is grid points with more precipitation in ICON-Sapphire than any of the MPI-ESM1.2-LR ensemble members.

All in all, the general response of radiation, temperature and precipitation to CO₂ in ICON-Sapphire is to first order surprisingly similar to that in MPI-ESM1.2-LR, given the different nature of the models. There are however intriguing differences such as the stronger surface temperature patterns are interesting in that they could explain some biases common to contemporary climate models (e.g. Zhou et al. (2016)), and the results for precipitation suggestive of a sharpening of the ITCZ in a warming world. The use of an ensemble for the lower resolution model appears promising, and suggests that already with a few years simulations with CO₂ forcing in ICON-Sapphire more firm conclusions regarding feedback mechanisms and other possible differences can be drawn.

4 Concluding remarks

The advances demonstrated here in both developing and utilising a coupled cloud- and ocean eddy-resolving Earth system model represents an important step towards leveraging exascale computing systems that will emerge in the coming years for weather and climate studies. As we have shown, super computing systems are at the verge of being able to run global simulations at the kilometre scale with a throughput of several months up to nearly a year per day. Thereafter, such simulations will become cheaper, but not faster. Hence, we argue, the time to develop these models is now.

Unlike previous incremental improvements from climate model resolution increases, the move to kilometre scale resolutions represents a step change. By simulating, rather than parameterising,

416 moist convection, gravity waves and ocean eddies using the equations of motion we are able to make
the model codes simpler and the results easier to understand, thereby injecting us with a genuine
418 hope of gaining new insights in years to come. Beyond advances in scientific understanding, the
implementation of kilometre resolution models at scale can bring climate science much closer to
420 users of climate change information by acting as so-called digital twins to Earths weather and
climate. For instance the local impacts of climate change, such as extremes of precipitation, storms
422 and droughts which are hardly represented in a meaningful way by current climate models can be
simulated directly with such models.

424 Another way in which these models can be useful is by testing whether they provide results that
are out of sample relative to contemporary climate models. We provided such an example with the
426 fast response to quadrupled CO₂, whereby a single expensive experiment with ICON-Sapphire was
compared to a computationally inexpensive ensemble with the CMIP6 class model MPI-ESM1.2-LR.
428 The purpose of the ensemble is to assess whether the single ICON-Sapphire experiment is within
the range of internal variability of MPI-ESM1.2-LR. Our initial investigations, based on an early
430 version of ICON-Sapphire, did not provide strong evidence of out of sample behavior relative to
MPI-ESM1.2-LR despite the vast difference in resolution and parameterisation. What we do find
432 is different is that the fast response of surface temperature and precipitation is more diverse in
ICON-Sapphire, with a larger representation of both weak and strong warming, as well as strong
434 increases in precipitation.

An important challenge is to limit model drifts to levels that are acceptable for the envisioned
436 purposes of the model, something which is usually done by tuning the radiation balance using pa-
rameters that are related to cloud processes. However, at kilometre scale resolutions the convection
438 parameterisation can be turned off, reducing the number of parameters, and at the same time the
parameters which remain are less uncertain. Therefore model developers may face situations where
440 they have to work with parameters outside their estimated range of uncertainty. In our case, for-
tunately, the radiation balance was already quite close to the observed, and minimal tuning was
442 necessary. Instead, we found in several instances that model physics changes, such as the turbu-
lence mixing schemes in both the ocean and atmosphere had large impacts on model drifts. It is
444 our hope that other institutes that are also pursuing global cloud resolving models can benefit from
some of our experiences.

446 **Acknowledgements** This work is supported by the Max-Planck-Gesellschaft (MPG). TM acknowl-
edges funding from the European Research Council (ERC) (Grant agreement No.770765) and the Eu-
448 ropean Union's Horizon 2020 research and innovation program projects CONSTRAIN and NextGEMS
(Grant agreements No.820829 and No.101003470). Computational resources were made available by
450 Deutsches Klimarechenzentrum (DKRZ) in Hamburg through support from Bundesministerium für
Bildung und Forschung (BMBF), by the the Gauss Centre for Supercomputing e.V. on the supercom-
452 puter JUWELS-Booster at the Jülich Supercomputing Centre (JSC), and by the Swedish National
Infrastructure for Computing (SNIC) at the National Supercomputing Centre (NSC) in Linköping
454 partially funded by the Swedish Research Council through grant agreement no. 2018-05973.

References

- 456 Amdahl, G.M. 1967. Validity of single processor approach to achieving large scale computing capabilities. *AFIPS Conference Proceedings*, 30, 483–485.
- 458 Armour, K. C., Bitz, C. M., and Roe, G. H. 2013. Time-Varying Climate Sensitivity from Regional Feedbacks, *Journal of Climate*, 26(13), 4518–4534.
- 460 Balaji, V. et al. 2022. Are GCMs obsolete? Manuscript submitted.
- Baldauf, M., Seifert, A., Foerstner, J., Majewski, D., Raschendorfer, M., and Reinhardt, T. 2011. Operational convective-scale numerical weather prediction with the COSMO model: Description and sensitivities. *Monthly Weather Review*, 139(12), 3887–3905.
- 464 Bjerknes, V. 1904. Das Problem der Wettervorhersage, betrachtet vom Standpunkte der Mechanik und der Physik. *Meteorol. Z.* 21, 1–7.
- 466 Bolin, B. 1955. Numerical forecasting with the barotropic model. *Tellus*, 7, 27–49.
- Bony, S., Bellon, G., Klocke, D. et al. 2013. Robust direct effect of carbon dioxide on tropical circulation and regional precipitation. *Nature Geosci* 6, 447–451, <https://doi.org/10.1038/ngeo1799>.
- Bony, S., Stevens, B., Ament, F. et al. 2017. EUREC4A: A Field Campaign to Elucidate the Couplings Between Clouds, Convection and Circulation. *Surv Geophys* 38, 1529–1568, <https://doi.org/10.1007/s10712-017-9428-0>.
- 472 Cess, R. D. et al. 1989. Interpretation of cloud-climate feedback as produced by 14 atmospheric general circulation models. *Science*, 245, 513–516.
- 474 Charney, J. G, Fjörtoft, R. and von Neumann, J. 1950. Numerical integration of the barotropic vorticity equation. *Tellus*, 2(4), 237–254.
- 476 Deardorff, J. 1970. A numerical study of three-dimensional turbulent channel flow at large Reynolds numbers. *Journal of Fluid Mechanics*, 41(2), 453–480. doi:10.1017/S0022112070000691.
- 478 Dipankar, A., Stevens, B., Heinze, R., Moseley, C., Zängl, G., Giorgetta, M., and Brdar, S. 2015. Large eddy simulation using the general circulation model ICON, *J. Adv. Model. Earth Syst.*, 7, 963–986, doi:10.1002/2015MS000431.
- 480 Fiedler, S., T. Crueger, R. D’Agostino, et al. 2020. Simulated Tropical Precipitation Assessed across Three Major Phases of the Coupled Model Intercomparison Project (CMIP). *Mon. Wea. Rev.*, 148, 3653–3680, doi:10.1175/MWR-D-19-0404.1.
- 484 Flynn, C. and Mauritsen, T. 2020 On the climate sensitivity and historical warming evolution in recent coupled model ensembles. *Atmos. Chem. Phys.* 20, 7829–7842, <https://doi.org/10.5194/acp-20-7829-2020>.
- 486

- 488 Fuhrer, O., Chadha, T., Hoefler, T., Kwasniewski, G., Lapillonne, X., Leutwyler, D., Lüthi, D., Osuna,
C., Schär, C., Schulthess, T. C., and Vogt, H. 2018: Near-global climate simulation at 1 km reso-
490 lution: establishing a performance baseline on 4888 GPUs with COSMO 5.0. *Geosci. Model Dev.*,
11, 1665–1681, <https://doi.org/10.5194/gmd-11-1665-2018>.
- 492 Giorgetta, M. A., Brokopf, R., Crueger, T., Esch, M., Fiedler, S., Helmert, J., C. Hohenegger, L. Korn-
blueh, M. Köhler, E. Manzini, T. Mauritsen, C. Nam, T. Raddatz, S. Rast, D. Reinert, M. Sakradzija,
494 H. Schmidt, R. Schneck, R. Schnur, L. Silvers, H. Wan, G. Zängl, B. Stevens, 2018. ICON-A, the at-
mosphere component of the ICON Earth system model: I. Model description. *Journal of Advances
in Modeling Earth Systems*, 10, 1613– 1637. <https://doi.org/10.1029/2017MS001242>.
- 496 Gregory, J. M., Ingram, W. J., Palmer, M. A., Jones, G. S., Stott, P. A., Thorpe, R. B., Lowe, J. A.,
Johns, T. C., and Williams, K. D. 2004. A new method for diagnosing radiative forcing and climate
498 sensitivity, *Geophys. Res. Lett.*, 31, L03205, doi:10.1029/2003GL018747.
- Hanke, M., R. Redler, T. Holfeld and M. Yastremsky, 2016. YAC 1.2.0: new aspects for coupling
500 software in Earth system modelling, *Geosci. Model Dev.*, 9, 2755–2769. DOI: 10.5194/gmd-9-2755-
2016.
- 502 Hanke, M. and R. Redler, 2019. New features with YAC 1.5.0. Reports on ICON, No 3. DOI:
10.5676/DWD_pub/nwv/icon_003.
- 504 Heikes, R. H. and Randall, D. A. 1995a. Numerical integration of the shallow- water equations on a
twisted icosahedral grid. Part I: Basic design and results of tests. *Mon. Wea. Rev.*, 123, 1862–1880.
- 506 Heikes, R. H. and Randall, D. A. 1995b. Numerical integration of the shallow- water equations on
a twisted icosahedral grid. Part II: A detailed description of the grid and analysis of numerical
508 accuracy. *Mon. Wea. Rev.*, 123, 1881–1887.
- Heinze, R., Dipankar, A., Henken, C.C., Moseley, C., Sourdeval, O., Trömel, S., Xie, X., Adamidis,
510 P., Ament, F., Baars, H., Barthlott, C., Behrendt, A., Blahak, U., Bley, S., Brdar, S., Brueck, M.,
Crewell, S., Deneke, H., Di Girolamo, P., Evaristo, R., Fischer, J., Frank, C., Friederichs, P., Göcke,
512 T., Gorges, K., Hande, L., Hanke, M., Hansen, A., Hege, H.-C., Hoose, C., Jahns, T., Kalthoff,
N., Klocke, D., Kneifel, S., Knippertz, P., Kuhn, A., van Laar, T., Macke, A., Maurer, V., Mayer,
514 B., Meyer, C.I., Muppa, S.K., Neggers, R.A.J., Orlandi, E., Pantillon, F., Pospichal, B., Röber, N.,
Scheck, L., Seifert, A., Seifert, P., Senf, F., Siligam, P., Simmer, C., Steinke, S., Stevens, B., Wapler,
516 K., Weniger, M., Wulfmeyer, V., Zängl, G., Zhang, D. and Quaas, J. 2017. Large-eddy simula-
tions over Germany using ICON: a comprehensive evaluation. *Q.J.R. Meteorol. Soc.*, 143: 69–100.
518 <https://doi.org/10.1002/qj.2947>.
- Held, I. M., Winton, M., Takahashi, K., Delworth, T., Zeng, F., and Vallis, G. K. 2010. Probing the
520 Fast and Slow Components of Global Warming by Returning Abruptly to Preindustrial Forcing,
Journal of Climate, 23(9), 2418–2427.

- 522 Hohenegger C. and B. Stevens, 2018. The role of the permanent wilting point in controlling the spatial distribution of precipitation. *Proc. Natl. Acad. Sci.*, 115, 5692-5697,
524 doi:10.1073/pnas.1718842115.
- Hohenegger, C., L. Kornblueh, D. Klocke, T. Becker, G. Cioni, J. F. Engels, U. Schulzweida and B.
526 Stevens, 2020. Climate statistics in global simulations of the atmosphere, from 80 to 2.5 km grid
spacing. *J. Meteorol. Society Japan*, 98, 73–91, doi:10.2151/jmsj.2020-005.
- 528 Hohenegger, C., P. Korn, L. Linardakis, R. Redler, R. Schnur, P. Adamidis, J. Bao, S. Bastin, M.
Behraves, M. Bergemann, J. Biercamp, H. Bockelmann, R. Brokopf, N. Bruggemann, M. Esch,
530 G. George, M. A. Giorgetta, O. Gutjahr, H. Haak, M. Hanke, T. Jahns, J. Jungclaus, M. Kern, D.
Klocke, L. Kluft, L. Kornblueh, S. S. Kosukhin, C. Kroll, J. Lee, V. Luschow, T. Mauritsen, R. Müller,
532 A. K. Naumann, L. Paccini, S. Panos, D. Praturi, D. Putrasahan, S. Rast, T. Riddick, N. Roeber,
H. Schmidt, U. Schulzweida, H. Segura, R. Shevchenko, V. Singh, M. S. Specht, C. Stephan, J.-S.
534 von Storch, R. Vogel, C. Wengel, M. Winkler, F. Ziemann, B. Stevens, 2022. The ICON Sapphire
model: a climate modeling system designed for applications at kilo- and subkilometer scales. In
536 preparation.
- Hourdin, F., Mauritsen, T., Gettelman, A., Golaz, J., Balaji, V., Duan, Q., Folini, D., Ji, D., Klocke,
538 D., Qian, Y., Rauser, F., Rio, C., Tomassini, L., Watanabe, M., and Williamson, D. 2017. The Art
and Science of Climate Model Tuning, *Bulletin of the American Meteorological Society*, 98(3),
540 589–602.
- Hyder, P., Edwards, J., Allan, R.P. et al. 2018. Critical Southern Ocean climate model biases traced to
542 atmospheric model cloud errors. *Nature Communication* 9, 3625, <https://doi.org/10.1038/s41467-018-05634-2>.
- 544 Jungclaus, J. H., et al. 2021. The ICON Earth System Model Version 1.0. *Earth and Space Science*
Open Archive, doi:10.1002/essoar.10507989.1.
- 546 Klemp, J. B., Wilhelmson, R. B. 1978. The Simulation of Three-Dimensional Convective Storm Dynamics,
Journal of Atmospheric Sciences, 35(6), 1070–1096.
- 548 Korn, P. and L. Linardakis, 2018. A conservative discretization of the shallow-water equations on
triangular grid. *J. Comp. Phys.* 375, 871–900.
- 550 Loeb, N. G., D. R. Doelling, H. Wang, W. Su, C. Nguyen, J. G. Corbett, L. Liang, C. Mitrescu, F. G.
Rose, and S. Kato, 2018. Clouds and the Earth’s Radiant Energy System (CERES) Energy Balanced
552 and Filled (EBAF) Top-of-Atmosphere (TOA) Edition-4.0 Data Product. *J. Climate*, 31, 895-918, doi:
10.1175/JCLI-D-17-0208.1.
- 554 Lohmann, U., Roeckner, E. 1996. Design and performance of a new cloud microphysics
scheme developed for the ECHAM general circulation model. *Climate Dynamics* 12, 557–572,
556 <https://doi.org/10.1007/BF00207939>.

- 558 Lorenz, E. N. 1969. The predictability of a flow which possesses many scales of motion, *Tellus*, 21:3, 289–307, doi:10.3402/tellusa.v21i3.10086.
- 560 Lott, F. 1999. Alleviation of stationary biases in a GCM through a mountain drag parameterization scheme and a simple representation of mountain lift forces, *Mon. Wea. Rev.*, 127, 788–801.
- 562 Manabe, S., Smagorinski, J., Strickler, R. F. 1965. Simulated climatology of a general circulation model with a hydrological cycle. *Monthly Weather Review*, 93(12), 769–798.
- 564 Manabe, S., Bryan, K. 1969. Climate calculations with a combined ocean-atmosphere model. *Journal of Atmospheric Sciences*, 26(4), 786–789.
- 566 Mauritsen, T., Svensson, G., Zilitinkevich, S. S., Esau, I., Enger, L., and Grisogono, B. 2007. A Total Turbulent Energy Closure Model for Neutrally and Stably Stratified Atmospheric Boundary Layers, *Journal of the Atmospheric Sciences*, 64(11), 4113–4126.
- 568 Mauritsen, T., et al. 2012. Tuning the climate of a global model, *J. Adv. Model. Earth Syst.*, 4, M00A01, doi:10.1029/2012MS000154.
- 570 Mauritsen, T., Bader, J., Becker, T., Behrens, J., Bittner, M., Brokopf, R., et al. 2019. Developments in the MPI-M Earth System Model version 1.2 (MPI-ESM1.2) and its response to increasing CO₂. *Journal of Advances in Modeling Earth Systems*, 11, 998–1038. <https://doi.org/10.1029/2018MS001400>.
- 572
- 574 Mauritsen, T., and Roeckner, E. 2020. Tuning the MPI-ESM1.2 global climate model to improve the match with instrumental record warming by lowering its climate sensitivity. *Journal of Advances in Modeling Earth Systems*, 12, e2019MS002037. <https://doi.org/10.1029/2019MS002037>.
- 576
- Moore, G. E. 1965. Cramming more components onto integrated circuits. *Electronics Magazine*, 38.
- 578 Morice, C.P., Kennedy, J.J., Rayner, N.A., Winn, J.P., Hogan, E., Killick, R.E., Dunn, R.J.H., Osborn, T.J., Jones, P.D., and Simpson, I.R. 2021. An updated assessment of near-surface temperature change from 1850: the HadCRUT5 dataset. *Journal of Geophysical Research*. doi:10.1029/2019JD032361.
- 580
- Palmer, T. and B. Stevens, 2019. The scientific challenge of understanding and estimating climate change. *Proc. Natl. Acad. Sci.* 116 (49) 24390–24395.
- 582
- Phillips, N.A. 1956. The general circulation of the atmosphere: A numerical experiment. *Q.J.R. Meteorol. Soc.*, 82: 123–164, doi:10.1002/qj.49708235202.
- 584
- Pithan, F., W. Angevine, and T. Mauritsen, 2015. Improving a global model from the boundary layer: Total turbulent energy and the neutral limit Prandtl number, *J. Adv. Model. Earth Syst.*, 07, doi:10.1002/2014MS000382.
- 586
- 588 Radtke, J., Mauritsen, T., and Hohenegger, C. 2021. Shallow cumulus cloud feedback in large eddy simulations – bridging the gap to storm-resolving models, *Atmos. Chem. Phys.*, 21, 3275–3288, <https://doi.org/10.5194/acp-21-3275-2021>.
- 590

- 592 Retsch, M. H., Mauritsen, T., and Hohenegger, C. 2019. Climate change feedbacks in aqua-
planet experiments with explicit and parametrized convection for horizontal resolutions
of 2,525 up to 5 km. *Journal of Advances in Modeling Earth Systems*, 11, 2070–2088,
594 <https://doi.org/10.1029/2019MS001677>.
- Richardson, L. F. 1922. *Weather prediction by numerical process*. Cambridge University Press, 258
596 pp.
- Röber, N., Böttinger, M., Stevens, B. 2021. Visualization of Climate Science Simulation Data. *IEEE
598 Computer Graphics and Applications*, 41(1), 42-48, doi: 10.1109/MCG.2020.3043987.
- Satoh, M. 2014. *Atmospheric Circulation Dynamics and General Circulation Models*. Springer Ver-
600 lag Heidelberg, doi:10.1007/978-3-642-13574-3.
- Schneider, T., Lan, S., Stuart, A., Teixeira, J. 2017. Earth system modeling 2.0: A blueprint for models
602 that learn from observations and targeted high-resolution simulations. *Geophysical Research
Letters*, 44, 12396–12417, doi:10.1002/2017GL076101.
- 604 Shepherd, T. 2014. Atmospheric circulation as a source of uncertainty in climate change projections.
Nature Geosci 7, 703–708, <https://doi.org/10.1038/ngeo2253>.
- 606 Smith, R.D., Maltrud, M.E., Bryan, F., Hecht, M.W. 2000. Numerical simulation of the North Atlantic
Ocean at $1/10^\circ$. *Journal of Physical Oceanography* 30, 1532–1561.
- 608 Stevens, B., Satoh, M., Auger, L. et al. 2019. DYAMOND: the DYnamics of the Atmospheric
general circulation Modeled On Non-hydrostatic Domains. *Prog Earth Planet Sci* 6, 61,
610 <https://doi.org/10.1186/s40645-019-0304-z>.
- Stevens, B., et al. 2021 EUREC4A, *Earth Syst. Sci. Data*, 13, 4067–4119, [https://doi.org/10.5194/essd-
612 13-4067-2021](https://doi.org/10.5194/essd-13-4067-2021).
- Sundqvist, H., Berge, E., and Kristjánsson, J. E. 1989. Condensation and Cloud Parameterization
614 Studies with a Mesoscale Numerical Weather Prediction Model, *Monthly Weather Review*, 117(8),
1641–1657.
- 616 Tiedtke, M. 1989. A comprehensive mass flux scheme for cumulus parameterization in large-scale
models. *Mon. Wea. Rev.* 117, 1779–1800.
- 618 Tomita, H., Tsugawa, M., Satoh, M., and Goto, K. 2001. Shallow water model on a modified icosahed-
hedral geodesic grid by using spring dynamics. *J. Comp. Phys.*, 174, 579–613.
- 620 Tomita, H., Satoh, M., and Goto, K. 2002. An optimization of icosahedral grid modified by spring
dynamics. *J. Comp. Phys.*, 183, 307–331.
- 622 Tomita, H., Miura, H., Iga, S., Nasuno, T., Satoh, M. 2005. A global cloud-resolving simulation: Pre-
liminary results from an aqua planet experiment. *Geophys. Res. Lett.* 32(8):3283.

- 624 Wan, H., Rasch, P. J., Zhang, K., Qian, Y., Yan, H., and Zhao, C. 2014. Short ensembles: an efficient
method for discerning climate-relevant sensitivities in atmospheric general circulation models,
626 *Geosci. Model Dev.*, 7, 1961–1977, <https://doi.org/10.5194/gmd-7-1961-2014>.
- Wang, C., Zhang, L., Lee, S.K., Wu, L., Mechoso, C.R. 2014. A global perspective on CMIP5 climate
628 model biases. *Nature Climate Change* 4, 201–205, <https://doi.org/10.1038/nclimate2118>.
- Washington, W. M., L. Buja, A. Craig, 2008. The computational future for climate and Earth system
630 models: on the path to petaflop and beyond. *Phil. Trans. R. Soc. A*.367833–846.
- Weller, H., H.G. Weller, and A. Fournier, 2009. Voronoi, Delaunay, and Block-Structured Mesh Re-
632 finement for Solution of the Shallow-Water Equations on the Sphere. *Mon. Wea. Rev.*, 137, 4208–
4224, doi:10.1175/2009MWR2917.1.
- 634 Winton, M., Takahashi, K., and Held, I. M. 2010. Importance of Ocean Heat Uptake Efficacy to
Transient Climate Change, *Journal of Climate*, 23(9), 2333–2344.
- 636 Yashiro, H., Terai, M., Yoshida, R., Iga, S.-I., Minami, K., and Tomita, H. 2016. Performance Anal-
ysis and Optimization of Nonhydrostatic ICosahedral Atmospheric Model (NICAM) on the K
638 Computer and TSUBAME2.5, in: *Proceedings of the Platform for Advanced Scientific Comput-
ing Conference on ZZZ – PASC’16*, ACM Press, <https://doi.org/10.1145/2929908.2929911>.
- 640 Zelinka, M. D., Myers, T. A., McCoy, D. T., Po-Chedley, S., Caldwell, P. M., Ceppi, P., et al.
2020. Causes of higher climate sensitivity in CMIP6 models. *Geophysical Research Letters*, 47,
642 e2019GL085782. <https://doi.org/10.1029/2019GL085782>.
- Zhou, C., Zelinka, M. and Klein, S. 2016. Impact of decadal cloud variations on the Earth’s energy
644 budget. *Nature Geosci* 9, 871–874, <https://doi.org/10.1038/ngeo2828>
- Zuidema, P., Chang, P., Medeiros, B., Kirtman, B. P., Mechoso, R., Schneider, E. K., Toniazzo, T.,
646 Richter, I., Small, R. J., Bellomo, K., Brandt, P., de Szoeki, S., Farrar, J. T., Jung, E., Kato, S., Li,
M., Patricola, C., Wang, Z., Wood, R., and Xu, Z. 2016. Challenges and Prospects for Reducing
648 Coupled Climate Model SST Biases in the Eastern Tropical Atlantic and Pacific Oceans: The U.S.
CLIVAR Eastern Tropical Oceans Synthesis Working Group, *Bulletin of the American Meteorolo-
650 gical Society*, 97(12), 2305–2328.